Dual Transport Systems Based on Hybrid Nanostructures of Microtubules and Actin Filaments

*Dong Shin Choi, Kyung-Eun Byun, and Seunghun Hong**

Motor proteins are highly efficient engines that convert the chemical energy of adenosine triphosphate (ATP) into mechanical energy.[1] Two representative motor proteins, kinesin and myosin, interact with different cytoskeletal elements, microtubules (MTs) and actin filaments (AFs), respectively. Thanks to the development of in-vitro assays for those proteins, motor proteins have been extensively studied and considered as a basic building block for nanotransportation devices.[2–5] For example, either MTs on kinesin or AFs on myosin have been utilized as a nanoshuttle that can carry various nanostructures such as viruses,[6,7] DNAs,[8–10] quantum dots,[11–13] and nanoparticles.[14] Transportation devices based on each motor protein have different advantages. MTs on kinesin tend to move straight, due to its rigid structure, and AFs on myosin have rather curved trajectories with fast gliding speeds. Therefore, kinesin-based devices are suitable for stable transportation over a long distance, while myosin-based ones can be useful in picking up cargo in highly miniaturized, curved tracks.[2,15,16] Although the necessity of an integrated device including both motor proteins has been addressed before,[2] kinesin and myosin motor proteins were believed to be incompatible, and previous nanotransportation systems based on MTs or AFs have been investigated exclusively either on kinesin or myosin. Such incompatibility between the two motor protein systems lowered the flexibility of device design and eventually limited the possible applications of protein motor-based nanotransport systems.

Herein, we develop microtubule–actin filament (MT–AF) hybrid nanostructures which can work as a nanotransportation system on both kinesin- and myosin-coated surfaces. In this work, the MT–AF hybrid nanostructures are constructed by conjugating MTs and AFs with biotin–streptavidin bonds. The motility of the MT–AF hybrid nanostructures is successfully demonstrated on both kinesin- and myosin-coated surfaces. Interestingly, the analysis of their trajectories reveals that the MT–AF hybrid nanostructures exhibited AF- or MT-like motions on myosin or kinesin, respectively. This hybrid nanostructure can be a simple but versatile platform for developing a nanotransportation system that can take advantage of these two different motor proteins.

Figure 1 illustrates the procedure to prepare MT–AF hybrid nanostructures and perform their motility assay on kinesin and myosin (details in the Experimental Section). In brief, biotinylated MTs were first polymerized from biotin-conjugated tubulin (Figure 1A). The MTs were then applied to a centrifugal column (YM-100, Millipore Corporation) for streptavidin conjugation. The MTs were bound to the membrane during streptavidin conjugation, which effectively prohibits the MTs from forming unwanted aggregates. After collecting the streptavidin-coated MTs from the column, the biotinylated AFs were mixed with the streptavidin-coated MTs to form MT–AF hybrid nanostructures. The motility assay of MT–AF hybrid nanostructures was performed on solid substrates coated with two different motor proteins: kinesin (Figure 1B) and myosin (Figure 1C). Here, chimera kinesin, NKHK560cys and rabbit skeletal myosin II were prepared and utilized for the motility assay as described previously.[17,18] For both motor protein systems, we used bovine serum albumin (BSA) as a blocking agent and BRB80 (80 mM piperazine-N,N′-bis (2-ethanesulfonic acid) (PIPES), 1 mM $MgCl_2$, 1 mM ethylene glycol tetraacetic acid (EGTA)) as a base buffer. This simple but efficient strategy allowed us to prepare MT–AF hybrid nanostructures which exhibit high motility on both kinesin- and myosin-coated surfaces.

Figure 2 shows the fluorescent images of the MT–AF hybrid nanostructures and some undesirable structures after the conjugation process of MTs and AFs. The MTs (red) were labeled with rhodamine, while the AFs (green) were labeled with fluorescein isothiocyanate (FITC). Figure 2A shows MT–AF hybrid nanostructures prepared by our method. Note that some MTs overlapped on top of AFs, indicating the formation of MT–AF hybrid nanostructures (highlighted by white dotted circles). The fluorescence microscopy analysis

Prof. S. Hong
Department of Physics and Astronomy
Seoul National University
Seoul, 151–747, Korea
E-mail: seunghun@snu.ac.kr
Prof. S. Hong
WCU Program
Department of Biophysics and Chemical Biology
Seoul National University
Seoul, 151–747, Korea
Prof. S. Hong
Department of Nano Science and Engineering
Seoul National University
Seoul, 151–747, Korea
D. S. Choi
Department of Nano Science and Engineering
Seoul National University
Seoul, 151–747, Korea
K.-E. Byun
Department of Physics and Astronomy
Seoul National University
Seoul, 151–747, Korea

DOI: 10.1002/smll.201002267

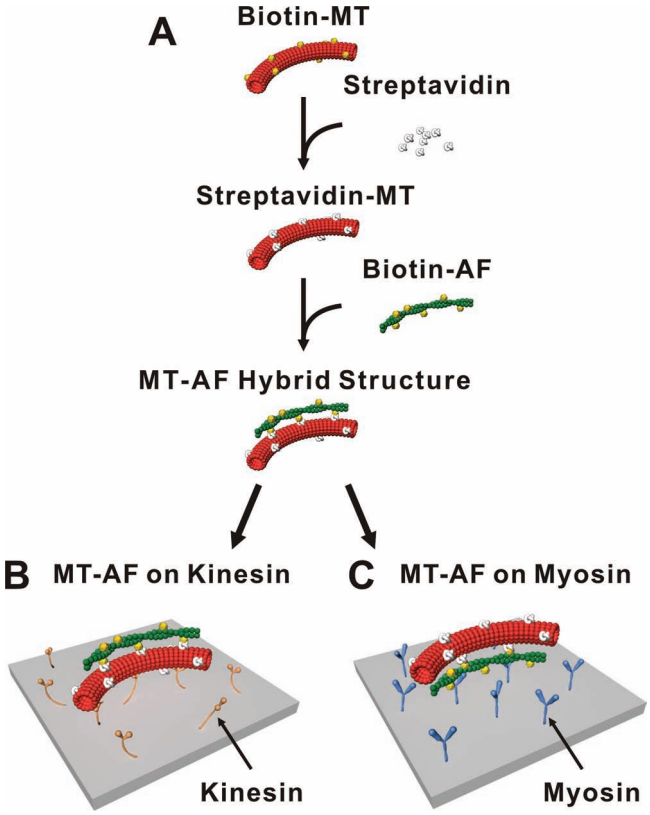

Figure 1. Schematic diagrams showing the synthesis process and the motility assay of MT–AF hybrid nanostructures. A) Building an MT–AF hybrid nanostructure. The biotinylated MTs were conjugated with streptavidin. Then, the biotinylated AFs were engaged with the MTs to obtain MT–AF hybrid nanostructures. B) Motility assay of an MT–AF hybrid nanostructure on a kinesin-coated surface. C) Motility assay of an MT–AF hybrid nanostructure on a myosin-coated surface.

shows that 32.4% or 34% out of 1082 MTs and 1033 AFs formed MT–AF hybrid structures. This yield may be further improved via various reported purification methods such as two sequential steps of cosedimentation assay with myosin and kinesin.[17,19] We performed the analysis to estimate the persistence length of these hybrid structures using the fluorescence microscopy images via the method reported previously (Supporting Information (SI), Figure S2A,B).[20] Here, the shape of filaments was considered as the series of unit vectors, and their persistence length was calculated using the cosine correlation function. The persistence length values measured from 167 MT–AF hybrid nanostructures had some distribution with its averaged value of 159.35 μm (SI, Figure S2C), which was smaller than that of MTs and larger than that of AFs.[21,22] It is also interesting to note that as the ratio of MTs in MT–AF hybrid nanostructures was increased, the overall persistence length of the MT–AF hybrid nanostructures was increased (SI, Figure S2D). Presumably, since the MT and the AF on a hybrid structure were not perfectly overlapped, some part of the MT or the AF was exposed freely without binding to the other filament (SI, Figure S2A,B). The unbound AF parts may allow MT–AF hybrid nanostructures to have the intermediate physical properties of MTs and AFs.

For the successful formation of MT–AF hybrid nanostructures, the concentrations of MTs and streptavidin during the conjugation process of streptavidin to the MTs are critical (Figure 2B,C). For example, if the concentration of MTs is very high on the membrane of the centrifugal column, the streptavidin often crosslinks several MTs together rather than coating individual MTs. Figure 2B shows that the excess MTs were crosslinked to each other and aggregated at a rather high concentration of MTs (≈0.8 μM of tubulin in BRB80 buffer). On the other hand, if the streptavidin concentration is very low, the free biotin molecules on MTs are not fully covered with the streptavidin, resulting in MT aggregates. Figure 2C shows some 'nanospool' structures that appeared when the concentration of streptavidin was reduced from 40 pM to 4 pM. Presumably, the shortage of streptavidin left the free biotin on the MT, and thus the MTs could bind to each other to form the aggregated structures. These nanospool structures were also reported previously when conjugating cargo to the filaments using biotin–streptavidin binding.[3,8,9,23–26] However, nanospool structures of AFs or MT–AF hybrid

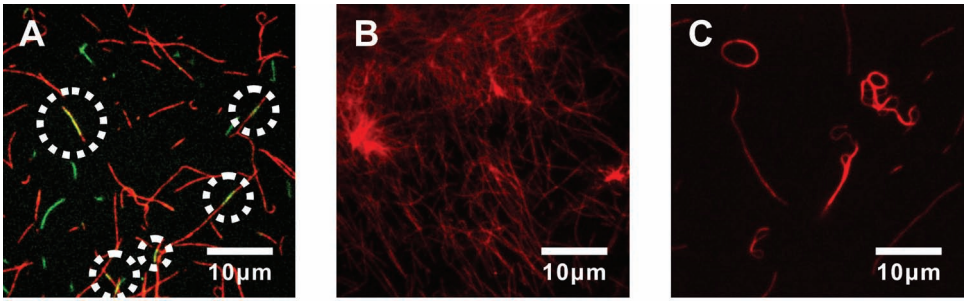

Figure 2. Fluorescence images of MT–AF hybrid nanostructures and some undesirable MT aggregates resulting from the conjugation processes. MTs and AFs are colored red and green, respectively. A) Individual MT–AF hybrid nanostructures (marked by white dotted circles) result from the process where 100 μL of biotinylated MT solution (tubulin concentration: 0.4 μM) was conjugated with 500 μL of 40 pM streptavidin solution in the centrifugal column and mixed with 100 μL of biotinylated AF solution (globular actin concentration: 0.4 μM). The conjugation process using solutions of these concentrations result in individual MT–AF hybrid nanostructures (marked by white dotted circles). B) MT aggregates result from the process using rather highly concentrated MT solution. Here, 100 μL of biotinylated MT (tubulin concentration: 0.8 μM) was conjugated with 500 μL of 40 pM streptavidin. Note that a rather high tubulin concentration results in MT aggregates. C) Nanospools and aggregates of MTs result from the process using rather low concentration streptavidin solution, as it leaves some unbound biotins on MTs. Here, 100 μL of biotinylated MT solution (tubulin concentration: 0.4 μM) was conjugated with 500 μL of 4 pM streptavidin solution.

NANO MICRO small

nanostructures were not observed in our experiments. Presumably, since AFs in the solution were coated only with biotin, they could not bind to each other to form nanospool structures. In the case of MT–AF hybrid nanostructures, biotinylated AFs bound to the streptavidin on the MTs to form the MT–AF nanostructures, and thus the free streptavidin density on the MT–AF hybrid nanostructures should have been very low. Therefore, it is expected that the MT–AF hybrid nanostructures hardly bound to each other to form nanospool structures.

The motions of the MT–AF hybrid nanostructures on kinesin- and myosin-coated surfaces are shown in **Figure 3**A,B, respectively (movies are available in the SI). The speed of the MT–AF hybrid nanostructure on kinesin was measured as ≈1.3 μm·s^{-1} (Figure 3A). In this case, kinesin and the MT (red) in the MT–AF hybrid nanostructures were regulating the movement of the AF (green) as a cargo. On the other hand, the speed of the MT–AF hybrid nanostructure on myosin was ≈2.4 μm·s^{-1} (Figure 3B). Here, the interaction between myosin and the AF transported the MT, even faster than MTs on kinesin. This result clearly shows that our MT–AF hybrid nanostructures can be transported on both kinesin- and myosin-coated substrates.

One of the key parameters to achieve high motility of MT–AF hybrid nanostructures on both motor proteins is the streptavidin coverage on MTs. For higher motility on kinesin-coated substrates, lower streptavidin coverage on the surface of individual MTs is preferred because the bound streptavidin on the MT surface may hinder the interaction between the kinesin and the MT.[27] On the other hand, higher streptavidin coverage on MTs is desirable for higher motility of the MT–AF hybrid nanostructure on myosin. It is because the skeletal myosin II used in this research is known to adhere strongly to MTs (SI, Figure S1).[28] When an MT–AF hybrid nanostructure encounters the myosin-coated surface, the myosin tends to adhere to the exposed MT in the MT–AF hybrid nanostructure and reduce its motility. To solve this problem, the streptavidin should cover the surface of the MT to hinder the attractive interaction between the MT and the myosin. However, some part of the MT should be exposed to interact with kinesin for the motility of the MT–AF hybrid nanostructure on kinesin. To determine the optimal streptavidin coverage on an MT during our preparation process, MT–AF hybrid nanostructures were prepared using MTs with different streptavidin coverages of 2%, 5%, 10%, and 25%, and an in-vitro motility assay was performed on kinesin or myosin using the prepared hybrid structures. We found that 5% streptavidin coverage on the MT resulted in optimal MT–AF hybrid nanostructures with a rather high motility on both kinesin- and myosin-coated solid substrates. When the streptavidin coverage was 2%, prepared MT–AF hybrid nanostructures did not move on the myosin. On the other hand, those prepared using the MTs with the streptavidin coverage of 10% or 25% exhibited little motility on kinesin.

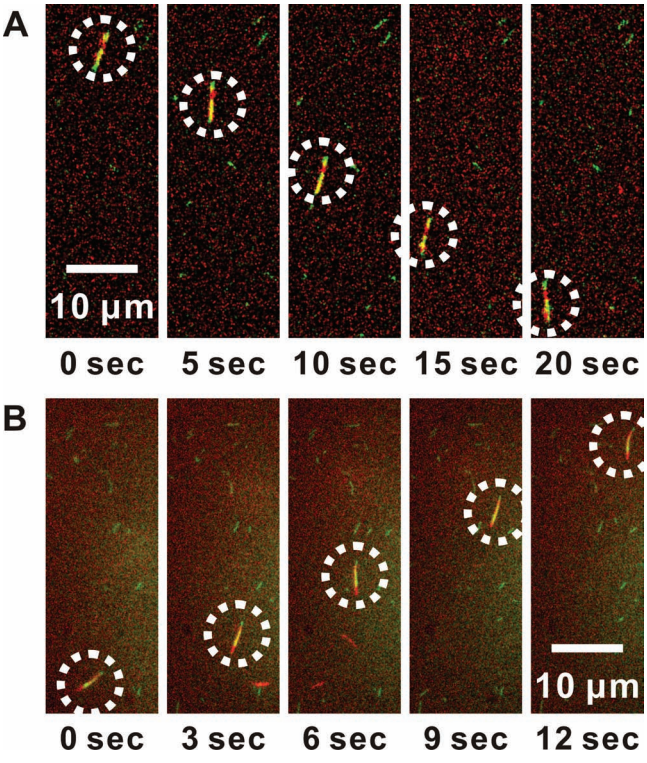

Figure 3. Time series of fluorescence images of MT–AF hybrid nanostructures (marked by white dotted circles) on A) kinesin and B) myosin. MTs and AFs are colored in red and green, respectively.

Figure 4A represents the speeds of the MT–AF hybrid nanostructures as well as MTs and AFs on either myosin or kinesin. These results show that the MT–AF hybrid nanostructures can be transported on both kinesin- and myosin-coated surfaces with a rather high speed of over 1 μm s^{-1}. However, the MT–AF hybrid nanostructures on myosin moved slower than the AFs on identical myosin. In addition, the speed of the MT–AF hybrid nanostructures was also slightly lower than that of the MTs on kinesin. One plausible explanation for the reduced motility of MT–AF hybrid nanostructures on myosin compared with AFs could be the strong attractive forces between MTs and myosin as reported previously (SI, Figure S1).[28] When an MT–AF hybrid nanostructure is moved by myosin motors on the substrates, other nearby myosin molecules could bind to some exposed parts of MTs in the MT–AF hybrid nanostructure and slow down its motion. Furthermore, the reduced motility of MT–AF hybrid nanostructures on both myosin and kinesin can also be attributed to the steric interference related to the rotational motion of AFs and MTs. Previous reports show that AFs and MTs often rotate during the motility assay.[12,13,29] Thus, all sides around the AFs or MTs should be accessible to myosin or kinesin, respectively, for a high motility. However, in the case of MT–AF hybrid nanostructures, one side of an MT (or AF) in it is blocked by AFs (or MTs) and, thus, is inaccessible to kinesin (or myosin) on the substrate, which should cause the steric interference and result in the reduced motility.[15,24,26,27,30] Since the speed of AFs highly depends on the number of myosin molecules binding to the AFs,[29] the steric hindrance should affect the motility of MT–AF hybrid nanostructures on myosin more than that on kinesin.

We performed a systematic analysis about the trajectories of each structure on two different motor proteins: AFs on myosin, MT–AF hybrid nanostructures on myosin, MT–AF hybrid nanostructures on kinesin, and MTs on kinesin. In

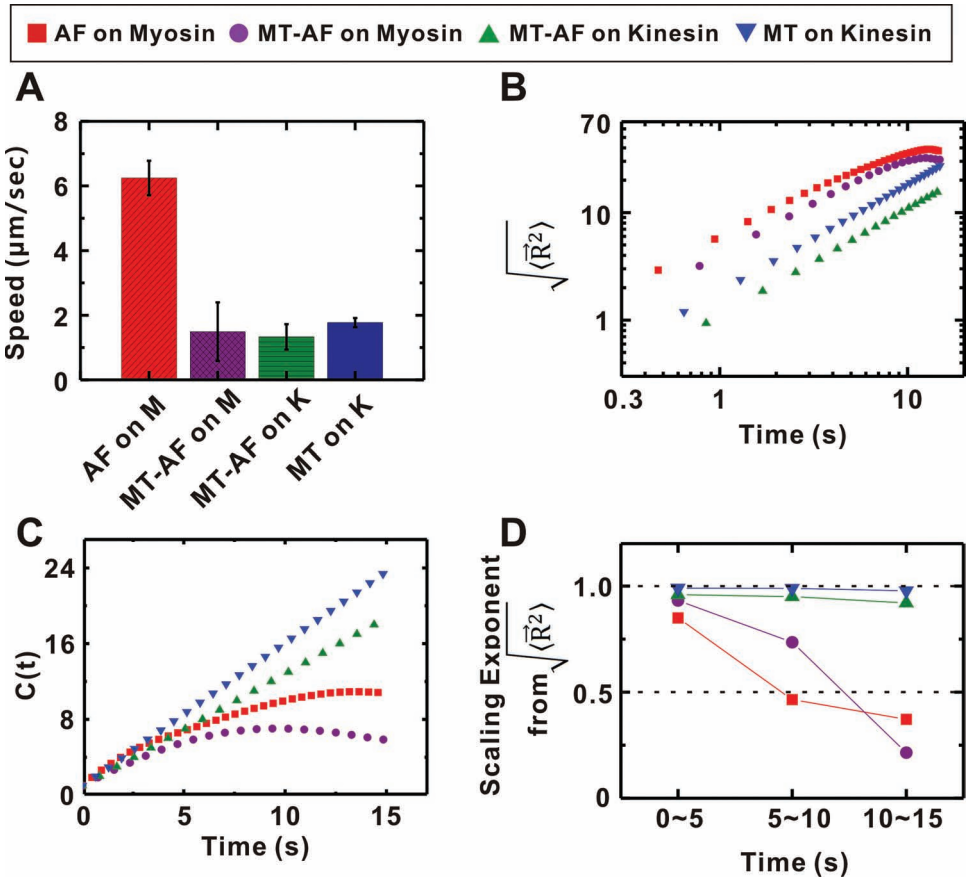

Figure 4. Analysis of the trajectories of AFs, MTs, and MT–AF hybrid nanostructures on kinesin and myosin. The plots with red, purple, green, and blue colors represent the data of AFs on myosin (M), MT–AF hybrid nanostructures on myosin, MT–AF hybrid nanostructures on kinesin (K), and MTs on kinesin, respectively. A) Average speed of AFs, MTs, and MT–AF hybrid nanostructures on kinesin or myosin. The error bars represent the standard deviations of the data. The averaged speed (the number n of averaged data) of AFs on myosin, MT–AF hybrid nanostructures on myosin, MT–AF hybrid nanostructures on kinesin, or MTs on kinesin were 6.4 ± 0.5 μm s^{-1} (n = 93), 1.5 ± 0.9 μm s^{-1} (n = 17), 1.3 ± 0.4 μm s^{-1} (n = 132), or 1.8 ± 0.1 μm s^{-1} (n = 132), respectively. B) Log–log plots of $\sqrt{\langle \vec{R}^2 \rangle}$ for typical trajectories. $\vec{R}$ represents the displacement vector from the initial position to the final position of AFs, MTs, or MT–AF hybrid nanostructures. The slopes for the trajectories on myosin decreased to ≈0.5 over time, indicating random diffusive motion. On the other hand, the graphs for the trajectories on kinesin exhibited a slope close to 1, implying rather straight motion. C) Averaged scaling exponents v calculated from $\sqrt{\langle \vec{R}^2 \rangle}$. The averaged data numbers are the same as those of (A). The v for the trajectories of filaments on myosin decreased to 0.5, indicating rather diffusive motion. On the other hand, that on kinesin remained as 1.0, indicating rather straight motion in that time period. D) Flory's characteristic ratio $C(t)$ for the trajectories of an AF, an MT, or an MT–AF hybrid nanostructures on kinesin or myosin. The $C(t)$ for the trajectories on the myosin saturated over time, indicating rather diffusive motion, while that on kinesin increased with a constant rate, indicating ballistic motion.

previous works, MTs and AFs were reported to move differently due to their different characteristics such as the stiffness of filaments and the duty ratio of motor proteins.[31] In general, AFs on myosin showed curved trajectories implying diffusive motions, while MTs on kinesin followed comparatively straight trajectories implying ballistic motions.[2,31] The difference in their trajectories can be quantitatively analyzed by introducing the vector $\vec{R}$ as reported previously.[32] In brief, the vector $\vec{R}$ is defined as the sum of the directional vectors along the trajectory, and it can also be referred to as the end-to-end vector of the trajectory for a given time period t. The characteristics of the trajectory can be analyzed by obtaining the scaling behavior of $\sqrt{\langle \vec{R}^2 \rangle}$ depending on the time period t like

$$\sqrt{\langle \vec{R}^2 \rangle} \approx t^{v}$$

where v is the scaling exponent varying usually from 0.5 to 1. We estimated the scaling exponent v by fitting the log–log plots of $\sqrt{\langle \vec{R}^2 \rangle}$ for the trajectories of AFs, MTs, and MT–AF hybrid nanostructures. In case of diffusive or ballistic motions, the scaling exponent should be 0.5 or 1, respectively.[33]

In Figure 4B, $\sqrt{\langle \vec{R}^2 \rangle}$ for typical trajectories of four different cases is shown in a log–log plot: an AF on myosin (red squares), an MT–AF hybrid nanostructure on myosin (purple circles), an MT–AF hybrid nanostructure on kinesin (green triangles), and an MT on kinesin (blue inverse triangles). Here, the slope of the log–log plots corresponds to the scaling exponent v of the corresponding trajectory at that time. Note that the scaling exponents of the trajectories for an MT and an MT–AF hybrid nanostructure on kinesin were close to 1 over the entire time period of the plot. On the other hand, those for an AF and an MT–AF hybrid nanostructure on myosin were close to 1 at the initial stage and then decreased to 0.5 over time. This indicates that the MT and the MT–AF hybrid nanostructure on kinesin performed ballistic motion

NANO MICRO small

over a rather long time period, while the AF and the MT–AF hybrid nanostructures on myosin performed ballistic motion at the initial stage and then became diffusive.

Figure 4C shows the averaged scaling exponent ν of $\sqrt{\langle \vec{R}^2 \rangle}$ for numerous trajectories of four different cases: AFs on myosin, MT–AF hybrid nanostructures on myosin, MT–AF hybrid nanostructures on kinesin, and MTs on kinesin. For a short time period (0–5 s), the trajectories for different cases had scaling exponents close to 1, indicating rather ballistic motion. However, the scaling exponents of the trajectories on myosin decreased to about 0.5, indicating diffusive motions, while those on kinesin remained close to 1 for a longer time (10–15 s).

The motion of the MT–AF hybrid nanostructures can also be analyzed using Flory's characteristic ratio $C(t)$ of the trajectories (Figure 4D). In brief, Flory's characteristic ratio represents the correlation between the directions of the initial and final portions of a trajectory.[32] For example, in case of a completely random motion without any directional correlation between the initial and final portions of its trajectory, $C(t)$ remains constant for a time period t. On the other hand, if the direction of the final portion of a trajectory is strongly correlated with that of an initial portion, $C(t)$ increases over time.[33] Note that $C(t)$ for the trajectories on myosin saturated to a constant value in a rather short time period (Figure 4D). This indicates that the motion on myosin exhibited rather diffusive characteristics, and the trajectories lost the directional correlations in a rather short time period. On the other hand, $C(t)$ for an MT or an MT–AF hybrid nanostructure on kinesin increased with a constant rate over time. It shows that the MT and the MT–AF hybrid nanostructure on kinesin kept their original directions over the time period. Practically, AFs and MT–AF hybrid nanostructures on myosin moved in trajectories with smaller radii of curvature than those of the MTs and MT–AF hybrid nanostructures on kinesin, resulting in rather straight trajectories.

We also estimated the scaling exponent ν from Flory's characteristic ratio (SI, Figure S3) and compared the results with the values estimated by the analysis of $\vec{R}$ (Figure 4C). Both analyses resulted in similar values of scaling exponents. Overall, these trajectory analyses clearly show that the motion of MT–AF hybrid nanostructures on myosin was more diffusive than that on kinesin.

It should be noted that although an MT–AF hybrid structure has a flexural rigidity between those of MTs and AFs, the structure on kinesin or myosin moves like an MT on kinesin or an AF on myosin. It implies that the characteristics of the MT–AF hybrid nanostructure's motion were mainly determined by the underlying motor protein rather than the rigidity of the filaments. A plausible explanation is that the different duty ratio of kinesin and myosin motor protein. In the case of kinesin, kinesin walks along the MT part of an MT–AF hybrid nanostructure, maintaining continuous attachment to the MT. On the other hand, since myosin transports an MT–AF hybrid nanostructure by tapping the AF part of the nanostructure, myosin can be detached from the filaments for a long time. Thus, MT–AF hybrid nanostructures on myosin can change their trajectory by thermal fluctuations more easily than those on kinesin. It is also worth discussing the effect of the flexural rigidity of the leading tip of MT–AF hybrid nanostructures. In previous work, the curvature of the trajectory of an MT on kinesin was attributed, in some degree, to the flexibility and the persistence length of the leading tip of the MT.[34] Since AFs and MTs in the hybrid structures were not perfectly overlapped, the unbound AFs or MTs at the end of the hybrid structure could work as leading tips and might affect the trajectories. However, in our experiments, the MT–AF hybrid structures with an MT as a leading tip exhibited similar curved tracks on myosin as those with an AF as a leading tip (SI, Figure S4). We obtained a similar result on kinesin substrates. Thus, the different curvatures of the tracks on myosin and kinesin can be attributed mostly to the duty cycle difference of myosin and kinesin motors rather than the flexibility difference between an AF and an MT.

In summary, we report MT–AF hybrid nanostructures that can function on both kinesin- and myosin-coated surfaces. By adjusting the streptavidin coverage on the MT surfaces to 5%, we were able to achieve motility of the MT–AF hybrid nanostructures on both kinesin- and myosin-coated surfaces with speeds of over 1 μm s^{-1}. From the analysis of their trajectories, an MT–AF hybrid nanostructure on kinesin or myosin behaves like an MT on kinesin or an AF on myosin. These unique properties of MT–AF hybrid structures may allow us to take advantage of both motor systems. Specifically, MT–AF hybrid structures on kinesin or myosin can move straight for stable cargo transportation or sweep narrow regions quickly for efficient cargo loading.[2] This hybrid nanostructure comprised of two different cytoskeletons can be a new versatile platform that can exploit the advantages from both motor protein systems and may pave the way for a complex nanotransportation system based on biological motors.

Experimental Section

Motor Protein Preparation: The chimera kinesin, NKHK560cys, was expressed in an *E. coli* system and purified with a His-tag (6× Histidine). The head and the neck domain of the *Neurospara crassa* kinesin, and the stalk of the *Homo sapiens* kinesin were constructed together with the His-tag, as reported previously.[18] The myosin was purified from rabbit skeletal muscle as described by Kron et al.[17] and utilized as the form of heavy meromyosin.

Preparation of the MT–AF Hybrid Nanostructure: We utilized commercially available tubulin and globular actin (Cytoskeleton, Inc.) for MTs and AFs. For the MT, the biotinylated tubulin (T333P) was polymerized as recommended in the provider's manual. It was mixed with the unlabeled tubulin (T240) and the rhodamine-labeled tubulin (TL590M) at the molar ratio of 5%. For the AF, the biotinylated globular actin (AB07) was polymerized with the globular actin (AKL99) at the molar ratio of 25% and stabilized with the Alexa Fluor 488 phalloidin (Invitrogen). To construct the MT–AF hybrid nanostructure, we first pre-coated the membrane of a centrifugal column (YM-100, Millipore) with casein solution (1 mg mL^{-1} in 10 mM Tris Buffer at pH 8.0) for better collection of the proteins. After immobilizing 100 μL of biotinylated MTs (tubulin concentration: 0.4 μM) on the membrane, the 500 μL of 40 pM streptavidin

solution was centrifuged in the column to conjugate streptavidin to the biotin on the MT surface. After washing off the remaining streptavidin from the top of the column, the streptavidin-coated MTs were collected in 100 μL of BRB80 buffer (80 mM PIPES, 1 mM $MgCl_2$, 1 mM EGTA). Finally, 100 μL of biotinylated AFs (globular actin concentration: 0.4 μM) and streptavidin-coated MTs were mixed together to form the MT–AF hybrid nanostructures.

Motility Assay: A conventional gliding assay[19,35] was used to observe the interaction of MTs, AFs, and MT–AF hybrid nanostructures with the motor proteins. Here, the motility buffer was modified so that we could use the identical motility conditions for both motor protein systems. The BSA was used as the blocking agent. All the buffers in contact with the MT were supplemented with 20 μM of Paclitaxel and kept at room temperature. To keep the same conditions for kinesin and myosin, BRB80 was used as the base buffer. The motility buffer contained 1 mM of ATP and 0.1% of methylcellulose.

Optics System: A fluorescence microscope (Nikon TE2000U) was utilized to observe the movement, and CoolLED (Custom Interconnect Ltd.) was used as the light source to illuminate differently labeled filaments. We analyzed the trajectories with Metamorph analysis software.

Supporting Information

Supporting Information is available from the Wiley Online Library or from the author.

Acknowledgements

This work was supported by the International Research & Development program (No. 2010–00293) and the NRF grant (No. 2010–0000799). SH acknowledges the support from the Converging Research Center Program (No. 2010K001138) and the WCU program.

[1] M. Schliwa, G. Woehlke, *Nature* **2003**, *422*, 759–765.
[2] T. Korten, A. Månsson, S. Diez, *Curr. Opin. Biotechnol.* **2010**, 477–488.
[3] A. Agarwal, H. Hess, *Prog. Polym. Sci.* **2010**, *35*, 252–277.
[4] A. Goel, V. Vogel, *Nat. Nanotechnol.* **2008**, *3*, 465–475.
[5] M. G. L. Van Den Heuvel, C. Dekker, *Science* **2007**, *317*, 333–336.
[6] G. Bachand, S. Rivera, A. Carroll-Portillo, H. Hess, M. Bachand, *Small* **2006**, *2*, 381–385.
[7] B. Martin, C. Soto, A. Blum, K. Sapsford, J. Whitley, J. Johnson, A. Chatterji, B. Ratna, *J. Nanosci. Nanotechnol.* **2006**, *6*, 2451–2460.
[8] S. Diez, C. Reuther, C. Dinu, R. Seidel, M. Mertig, W. Pompe, J. Howard, *Nano Lett.* **2003**, *3*, 1251–1254.
[9] C. Dinu, J. Opitz, W. Pompe, J. Howard, M. Mertig, S. Diez, *Small* **2006**, *2*, 1090–1098.
[10] S. Ramachandran, K. H. Ernst, G. Bachand, V. Vogel, H. Hess, *Small* **2006**, *2*, 330–334.
[11] G. D. Bachand, S. B. Rivera, A. K. Boal, J. Gaudioso, J. Liu, B. C. Bunker, *Nano Lett.* **2004**, *4*, 817–821.
[12] A. Mansson, M. Sundberg, M. Balaz, R. Bunk, I. A. Nicholls, P. Omling, S. Tagerud, L. Montelius, *Biochem. Biophys. Res. Commun.* **2004**, *314*, 529–534.
[13] B. Nitzsche, F. Ruhnow, S. Diez, *Nat. Nanotechnol.* **2008**, *3*, 552–556.
[14] F. Patolsky, Y. Weizmann, I. Willner, *Nat. Mater.* **2004**, *3*, 692–695.
[15] J. Howard, *Mechanics of motor proteins and the cytoskeleton*, Sinauer Associates, Sunderland, MA, **2001**.
[16] M. Sundberg, R. Bunk, N. Albet-Torres, A. Kvennefors, F. Persson, L. Montelius, I. A. Nicholls, S. Ghatnekar-Nilsson, P. Omling, S. Tagerud, A. Mansson, *Langmuir* **2006**, *22*, 7286–7295.
[17] S. J. Kron, Y. Y. Toyoshima, T. Q. P. Uyeda, J. A. Spudich, *Methods Enzymol.* **1991**, *196*, 399–416.
[18] C. T. Lin, M. T. Kao, K. Kurabayashi, E. Meyhöfer, *Small* **2006**, *2*, 281–287.
[19] I. Vernos, *Kinesin Protocols*, Humana Pr. Inc., Totowa, NJ **2001**.
[20] A. Ott, M. Magnasco, A. Simon, A. Libchaber, *Phys. Rev. E* **1993**, *48*, R1642–R1645.
[21] F. Gittes, B. Mickey, J. Nettleton, J. Howard, *J. Cell Biol.* **1993**, *120*, 923–934.
[22] F. Pampaloni, G. Lattanzi, A. Jonas, T. Surrey, E. Frey, E. L. Florin, *Proc. Natl. Acad. Sci. USA* **2006**, *103*, 10248–10253.
[23] H. Hess, J. Clemmens, C. Brunner, R. Doot, S. Luna, K.-H. Ernst, V. Vogel, *Nano Lett.* **2005**, *5*, 629–633.
[24] M. Bachand, A. M. Trent, B. C. Bunker, G. D. Bachand, *J. Nanosci. Nanotechnol.* **2005**, *5*, 718–722.
[25] H. Q. Liu, E. D. Spoerke, M. Bachand, S. J. Koch, B. C. Bunker, G. D. Bachand, *Adv. Mater.* **2008**, *20*, 4476–4481.
[26] R. Kawamura, A. Kakugo, Y. Osada, J. P. Gong, *Nanotechnology* **2010**, *21*, 145603–145614.
[27] T. Korten, S. Diez, *Lab Chip* **2008**, *8*, 1441–1447.
[28] L. Griffith, T. Pollard, *J. Cell Biol.* **1978**, *78*, 958.
[29] T. Q. P. Uyeda, S. J. Kron, J. A. Spudich, *J. Mol. Biol.* **1990**, *214*, 699–710.
[30] N. Suzuki, H. Miyata, S. Ishiwata, K. Kinosita Jr, *Biophys. J.* **1996**, *70*, 401–408.
[31] T. Nitta, A. Tanahashi, Y. Obara, M. Hirano, M. Razumova, M. Regnier, H. Hess, *Nano Lett.* **2008**, *8*, 2305–2309.
[32] K. E. Byun, K. Heo, S. Shim, H. J. Choi, S. Hong, *Small* **2009**, *5*, 2659–2664.
[33] H. Berg, *Random Walks in Biology*, Princeton Univ Press, Princeton, NJ, **1993**.
[34] M. G. L. Van Den Heuvel, S. Bolhuis, C. Dekker, *Nano Lett.* **2007**, *7*, 3138–3144.
[35] J. M. Scholey, *Motility Assays for Motor Proteins*, Academic Press, Inc., Vol. *39*, San Diego **1993**.

Received: December 15, 2010
Revised: March 22, 2011
Published online: May 12, 2011